ACES Asian Chemical Editorial Society

DOI: 10.1002/cnma.201700161

CHEMNANOMAT
Full Paper

Carbon Nanostructures

Improvement of the Structural and Chemical Properties of Carbon Nano-onions for Electrocatalysis

Olena Mykhailiv,[a] Halyna Zubyk,[a] Krzysztof Brzezinski,[a] Malgorzata Gras,[b] Grzegorz Lota,[b] Marianna Gniadek,[c] Elkin Romero,[d] Luis Echegoyen,[d] and Marta E. Plonska-Brzezinska*[a]

Abstract: Heteroatom doping of carbon nanostructures is a convenient tool to control their physicochemical properties and to make them suitable for various applications. Carbon nano-onions (CNOs) doped with nitrogen (N-CNOs) have been prepared by annealing aminated-nanodiamond particles (AM-NDs) at different temperatures (1150, 1450 and 1650 °C) in an inert He atmosphere. Their physicochemical properties were compared with those of pristine CNOs obtained from non-functionalized NDs under the same experimental conditions. The carbon nanostructures were characterized using transmission (TEM) and scanning (SEM) electron microscopy, X-ray powder diffraction (XRD), Raman and Fourier transform infrared (FTIR) spectroscopy, porosimetry, and differential-thermogravimetric analyses (TGA-DTG). Their physicochemical properties are systematically discussed for undoped and for the nitrogen-doped CNO samples. The results reveal that the surface morphology and the structure of undoped and nitrogen-doped CNOs vary with the annealing temperature. All of these materials were electrochemically tested as electrode materials for enzyme-free catalysis of hydrogen peroxide. The nitrogen-doped carbon nanostructures have a higher catalytic activity than undoped nanostructures obtained under the same experimental conditions.

Introduction

Carbon nano-onions (CNOs) are promising carbon nanostructures that consist of a multi-layered arrangement of closed fullerene shells.[1,2] The most practical, economical and by far the simplest procedure to prepare carbon nano-onions (5 nm, average size) was proposed by Kuznetzov.[3] This procedure involves the thermal annealing of nanodiamond particles (NDs) in a neutral gas atmosphere, leading to a progressive transformation of the carbon atom structure and formation of spherical CNOs with diameters ca. 5 nm. The structure of the CNOs obtained from ND particles, and their physical and electrical properties are a function of their synthesis procedure, mainly the annealing temperature.[4] Increasing the annealing temperature up to 1600 °C results in an increase of the density of states of conductive electrons.

Nitrogen-doped carbon nanostructures have shown interesting electrochemical and electrocatalytic properties and they are frequently used in energy and sustainability applications.[5] Carbon materials are frequently applied as electrodes for electric double layer capacitors (EDLC) or supercapacitors.[6–8] An EDLC is an electrochemical energy storage device with high power density and good cycling life,[9] in which the main parameter determining their electrochemical properties is their porous structure.[10,11] The mechanism for energy storage in EDLC is the separation of charges at the carbon electrode/electrolyte interface.[7] This process occurs very quickly compared with those in batteries, therefore, EDLCs reach high power rates. Unfortunately, the pure carbon materials have limited capacity to store electric charge. Therefore, a number of modifications have been introduced in order to improve their electrochemical parameters.[12–15] One of the commonly used methods is doping of the carbon structures with atoms with different electronic configurations, such as N, P, S, B, etc.[8,16]

N-doping can induce an n-type electronic modification as observed for typical semiconducting materials, which enables the potential use of these doped materials in multiple important nanoelectronic applications.[17] Nitrogen-doped carbon nanostructures may be applied as electrocatalysts in oxygen reduction reactions,[18–20] as electrochemical sensors and biosensors for hydrogen peroxide (H_2O_2),[5,21,22] and glucose,[23] and

[a] O. Mykhailiv, Dr. H. Zubyk, Dr. K. Brzezinski, Prof. M. E. Plonska-Brzezinska
Institute of Chemistry
University of Bialystok
Ciolkowskiego 1K, 15-245 Bialystok (Poland)
E-mail: mplonska@uwb.edu.pl

[b] M. Gras, Dr. G. Lota
Poznan University of Technology
Institute of Chemistry and Technical Electrochemistry
Berdychowo 4, 60-965 Poznan (Poland)

[c] Dr. M. Gniadek
Department of Chemistry
University of Warsaw
Pasteur 1, 02-093 Warsaw (Poland)

[d] E. Romero, Prof. L. Echegoyen
Department of Chemistry
University of Texas at El Paso
500 W. University Ave., El Paso, TX 79968 (USA)

Supporting information for this article can be found under: https://doi.org/10.1002/cnma.201700161.

as anode materials in Li-ion batteries.[17] H_2O_2 is a molecular metabolite that plays a vital role in the regulation of various physiological processes in living organisms[24] and is an important analyte in clinical diagnosis.[25]

We report herein an effective nitrogen-doping approach during the synthesis of CNOs to enhance their electrocatalytic properties. Attempts to synthesize nitrogen-doped onion-like structures or to modify CNO nanostructures with nitrogen atoms, mostly using post-modification (post-synthesis) methods, lead to the formation of many by-products and low reaction yield.[26–28] Such doped-nanostructures have been used in dye-sensitized solar cells,[29] as catalysts for epoxidation reactions[30] and in fuel cells.[26]

As the starting material, we used aminated-nanodiamond particles (AM-NDs, 5 nm in diameter) and heated them in an inert He atmosphere at high temperatures (1150, 1450 and 1650 °C) to obtain nitrogen-doped carbon nano-onions (N-CNOs). In our studies we also used undoped CNOs as reference nanostructures synthesized at the same temperatures. We also used the newly-synthesized materials for enzyme-free electrocatalysis.

Results and Discussion

Preparation and structural characterization of undoped and nitrogen-doped CNO

Commercially available AM-NDs with a crystal size between 4 and 6 nm were used for the preparation of nitrogen-doped CNOs (N-CNOs) (Figure 1 a). The central fullerene at the core of the CNOs is surrounded by multiple layers of nested concentric graphitic shells, with an intershell spacing estimated from the high-resolution transmission electron microscopy (HRTEM) diffraction patterns of around 0.34 nm, similar to that for highly oriented pyrolitic graphite (Figure 1 c). The standard procedure reveals spherical nanostructures composed of 6–11 layered CNOs (Figure 1). The synthesis was carried out at three different temperatures: 1150; 1450 and 1650 °C. At 1150 °C both samples (unmodified and aminated NDs), showed the formation of inhomogeneous nanoparticles with a core nanodiamond structures and outer graphitic layers (Figure 1 b). We did not observe any fundamental differences between structures obtained from NDs and AM-NDs under these experimental conditions. The highest temperatures led to the complete transformation of the NDs into the multilayered fullerenes (Figures 1 d and 1 e). The nitrogen doping process leads to the formation of polygonal and spherical nanostructures with the different diameters (Figure 1 e).

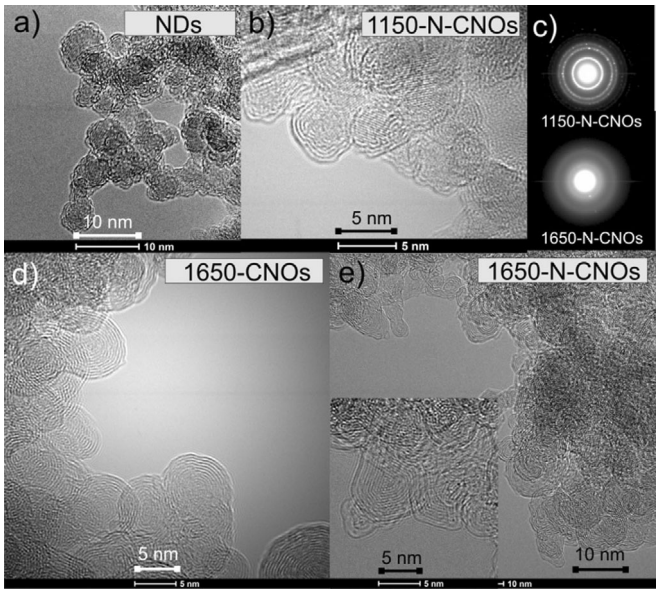

Figure 1. TEM studies of (a) NDs, (b) 1150-CNOs, (d) 1650-CNOs and (e) 1650-N-CNOs. (c) TEM diffraction patterns of 1150-N-CNOs and 1650-N-CNOs.

Our X-ray diffraction (XRD) investigation revealed the gradual transformation of diamond into graphite-like nanostructures as a function of the annealing temperature. XRD patterns for pristine NDs, AM-NDs, undoped CNOs and N-doped CNOs (the last two products obtained at: 1150, 1450 and 1650 °C) are shown in Figure 2. The XRD traces for CNOs and N-CNOs did not show significant differences. The ND and CNO profiles show the presence of a mixture of various phases. For the ND and AM-ND materials (Figure 2 a and Figure 2 e, respectively), the strongest peaks at 2θ of around 43.8° correspond to the (111) basal plane diffraction of the diamond structure.[31] A certain amount of a graphite-like and an amorphous phase ($2\theta =$ 21.5°) were also detected.[32,33] The conversion from nanodiamond to graphitized carbon nano-onions was observed during the annealing process of the starting material. For all samples an asymmetric second peak with a maximum at 43.0° were observed, that are attributed to the (002) and (100) planes of graphite, respectively (Figures 2 b–2 d and 2 f–2 h). The broad peaks centered around 23–27° with a maximum at 25.1° suggest contributions from some sp^2-bonded carbons in the CNO and N-CNO samples, and can be attributed to the different forms of carbon, turbostratic carbon (amorphous), graphene

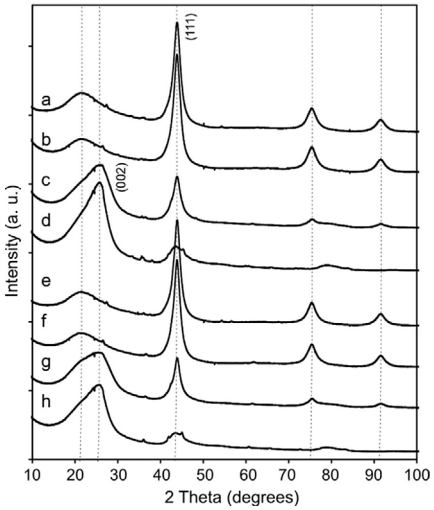

Figure 2. XRD studies of (a) NDs, (b) 1150-CNOs, (c) 1450-CNOs, (d) 1650-CNOs, (e) AM-NDs, (f) 1150-N-CNOs, (g) 1450-N-CNOs, and (h) 1650-N-CNOs.

carbon (graphitic carbon) and a hexagonal lattice characteristic for carbon nitride.[34–36] These peaks are relatively broad and weak. The diffraction broadening arises primarily from the size of the nanoparticles and can also be caused by strains and defects in the crystal material itself and by incompletely formed shells of CNOs.

Spectroscopic and thermogravimetric characteristics of CNOs and N-CNOs

Raman spectroscopy is one of the most informative techniques for the characterization of carbon nanostructures.[37,38] The Raman absorptions for NDs and CNOs and for their nitrogen-doped structures have been identified as the origin of the *D* and *G* peaks and of the second order the *D* peak.[39] The *G* and *D* peaks lie at around 1560 and 1360 cm^{-1} for visible excitation, respectively. The Raman spectra of carbon films are dominated by the sp^2 sites (*G* band). Only for diamond or samples containing a significant fraction of a diamond phase, the diamond sp^3 peak at 1332 cm^{-1} is observed (*D* band).[39] In the case of structures as the CNOs, both bands are present and depending on their position, shape, and relative intensities we can infer the number of graphitic layers in the structure, their structural modifications, and the degree of transformation of ND nanoparticles into spherical CNO structures. The ratio of the *D* and *G* band intensities (I_D/I_G and I_{2D}/I_G) is often used as a diagnostic tool to check the homogeneity of carbon nanostructures. To reveal the change in the position and intensity of Raman peaks the spectra were normalized to the intensity of the *G* band and fitted to the four Lorentz-shape components.[40] The obtained data are presented in Figure 3 and collected in Table 1.

Nanodiamonds are faceted polyhedral structures consisting of a diamond core built by sp^3 carbon atoms, a transition layer formed primarily by disordered sp^3 carbon atoms and a near surface transition region coated by a fullerene-like shell of sp^2 carbon atoms.[41,42] The presence of sp^2 and sp^3 carbon atoms is visible in the Raman spectra of NDs and AM-NDs on Figure 3a and Figure 3e, respectively. The main diamond absorptions are observed at 1320 cm^{-1} and as a broadened intense signal near 1600 cm^{-1}. The last one originates from the absorption of aromatic rings, from surface functional groups and adsorbed molecules.[37,41,43] Therefore, the Raman spectrum of AM-NDs is dominated by two bands with peak maxima near 560 and 1100 cm^{-1} (Figure 3e). The assignment of these two bands is not clear from the literature. The band at lower frequency is characteristic for nitrogenated carbon[44] or out-of-plane vibrations of sp^3 type C–C bonds.[45] This implies that the presence of nitrogen is able to support the formation of carbon sp^3 type bonds.[46] These two bands were also observed in the Raman spectra of nanophase diamond powder (broad peak at about 500 cm^{-1} and sharp peaks at 1090 cm^{-1}, using 514 nm laser excitation energies).[47] It is very important to note the absence of these two peaks in the NDs (Figure 3a), which confirms a more amorphous character of AM-NDs compared with NDs. These two bands are not present in the Raman spectra of carbon samples after annealing of the AM-NDs. Increasing disorder was also observed upon increased annealing temperature, reflected in the width of the *D* band and the I_D/I_G and I_{2D}/I_G ratios, which increase at higher annealing temperatures (Table 1). Kaufman et al. concluded that nitrogen substitution is responsible for the symmetry breaking of the E_{2g} mode and for the intensity of the *G* and *D* bands.[48]

Table 1. Best-fit frequencies for *D*, *G* and *2D* bands obtained at 514 nm laser excitation energies and relative intensity I_D/I_G and I_{2D}/I_G.

Sample	*D* band [cm^{-1}]	*G* band [cm^{-1}]	*2D* band [cm^{-1}]	I_D/I_G	I_{2D}/I_G
NDs	1320	1622	–	0.7	–
1150-CNOs	1348	1588	–	1.1	–
1450-CNOs	1333	1580	2661	1.22	0.46
1650-CNOs	1337	1576	2670	1.33	0.77
AM-NDs	1325	1601	–	0.55	–
1150-N-CNOs	1347	1582	–	0.74	–
1450-N-CNOs	1334	1582	2667	1.19	0.16
1650-N-CNOs	1336	1570	2666	1.47	0.90

The data for the three main bands (*D*, *G* and *2D*) for undoped and nitrogen-doped CNOs showed that the vibrational bands did not shifted significantly. It is important to note that the Raman spectrum for the undoped 1650-CNOs shows *D/G* and *2D/G* intensity ratios of 1.33 and 0.77, respectively (Table 1). The carbon nanostructures obtained under the same experimental conditions from AM-ND particles showed an increase of the intensity of the *D* and *2D* bands (1650-N-CNOs: $I_D/I_G = 1.47$ and $I_{2D}/I_G = 0.90$) as a result of the formation of the N–C bonds. The effect of nitrogen doping primarily leads to a systematic increase of the intensity of the disorder-induced band (*D* band).

The identification of the structural changes of CNOs during annealing and nitrogen-doping was monitored using Fourier transform infrared spectroscopy (FTIR). Figure S1 shows FTIR

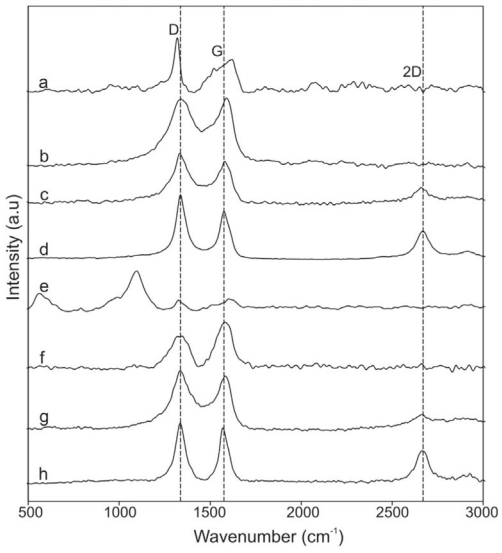

Figure 3. Raman (recorded at $\lambda_{ext} = 514$ nm) of (a) NDs, (b) 1150-CNOs, (c) 1450-CNOs, (d) 1650-CNOs, (e) AM-NDs, (f) 1150-N-CNOs, (g) 1450-N-CNOs, and (h) 1650-N-CNOs.

spectra of all samples (ND, AM-ND, CNO and N-CNO) and Table S1 presents the data for these samples. The NDs and AM-NDs have a common band in the range of 3660–3020 cm^{-1}, which can be assigned to the N–H deformation vibration of amine groups or the symmetric and asymmetric stretch vibrations of water molecules.[41] The peak near 1640 cm^{-1} derives from the O–H bending vibrations or the N–H deformation vibrations.[49] The bands at 2950–2920 cm^{-1} and 2810–2870 cm^{-1} correspond to stretching vibrations of C–H groups.[49] According to the literature, the bands at 1570–1540 can be assigned to the stretching of the C=N bonds or to the stretching of aromatic rings (C=C). Therefore, the peaks in the 1400–1000 cm^{-1} region (Table S1) are assigned to the C–N stretching or stretching modes of –OH groups.[49] Also, characteristic bands are observed at low frequencies, that can be assigned to C–N heteroring vibrations or out-of-plane bending modes of C–H and N–H.

Differential-thermogravimetric analysis (TGA-DTG), was performed to probe the thermal stability of undoped and nitrogen-doped CNOs (Figure 4 and Table S2). The pristine and aminated-nanodiamond particles were the reference samples. Figure 4 shows TGA-DTG scans in an air atmosphere for all analyzed samples. The degree of graphitization of the CNOs could be studied using thermogravimetric analysis, which shows that the higher the oxidation temperature the more homogeneously graphitized carbon structures are obtained.[50] The onset oxidation, inflection and end temperatures are listed in Table S2. These values represent the initial weight loss, the maximum weight loss and the final weight. The highest inflection temperatures were observed for the CNOs obtained at 1650 °C from pristine and AM-NDs (650 and 645 °C, respectively). In the first case, the temperature range between the onset and end temperatures is wider (ca. 100 °C), indicating a more polycrystalline character of the resulting CNO structures (1650-CNOs, see Table S2). In other words, the 1650-N-CNOs show more homogenous and highly graphitized nanostructures (ca. 55 °C, see Table S2), in agreement with the literature.[51] The nanostructures obtained at 1450 °C clearly show their transitional nature with two maxima (at 576 and 591 °C for 1450-CNOs and at 546 and 569 °C for 1450-N-CNOs), which are probably associated with the presence of NDs in the core and spherical graphene layers in the outer layers of the carbon nanoparticles.

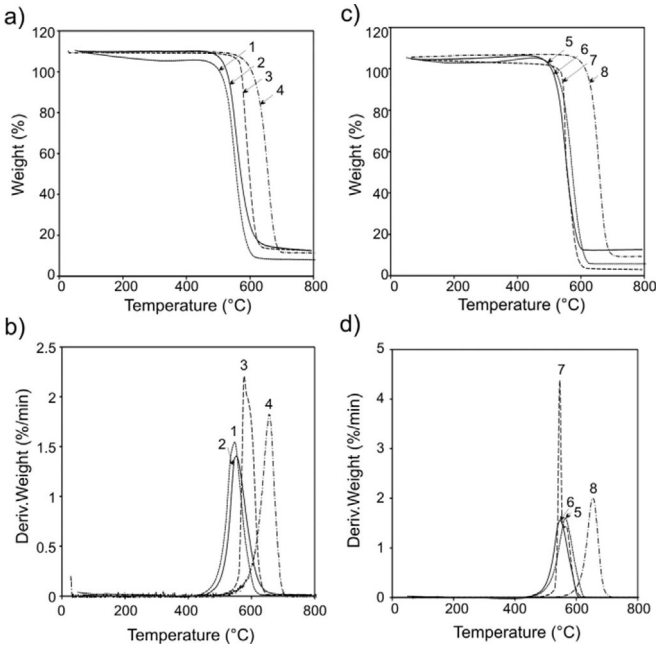

Figure 4. (a, c) TGA and (b, d) DTG curves for: (1) NDs, (2) 1150-CNOs, (3) 1450-CNOs, (4) 1650-CNOs, (5) AM-NDs, (6) 1150-N-CNOs, (7) 1450-N-CNOs, (8) 1650-N-CNOs in an air atmosphere at 10 °C min^{-1}.

Textural characteristics of CNOs and N-CNOs

Doping of carbon materials with nitrogen atoms affects their hydrophilicity and wettability, which in turn determines their dispersity in polar solvents (Figure S2). This relationship was also observed in our measurements performed using scanning electron microscopy (SEM). Comparison of carbon materials obtained at the same temperatures (Figure 5), indicates clearly that doping with nitrogen leads to smaller aggregates and to more uniform/homogenous films on the surfaces (dispersion of CNOs in ethanol on a Au foil).

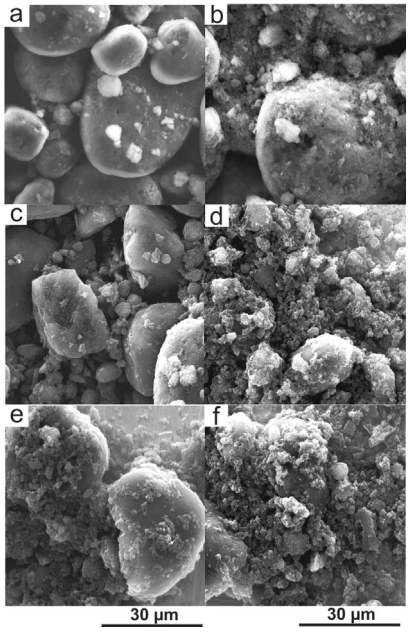

Figure 5. SEM images of the Au foil covered with (a) 1150-CNOs, (b) 1150-N-CNOs, (c) 1450-CNOs, (d) 1450-N-CNOs, (e) 1650-CNOs, and (f) 1650-N-CNOs.

Nitrogen-doping of carbon nano-onion structures altered their textural properties, in agreement with the gas adsorption measurements (Figure 6). The adsorption and desorption characteristics of nitrogen, the micro- and mesopore structure, the pore volume and the specific surface area of all types of CNOs were measured by a multilayer model of coverage adsorption, the Brunauer–Emmett–Teller (BET) static nitrogen adsorption technique (Figure 6). The highest specific surface area was ob-

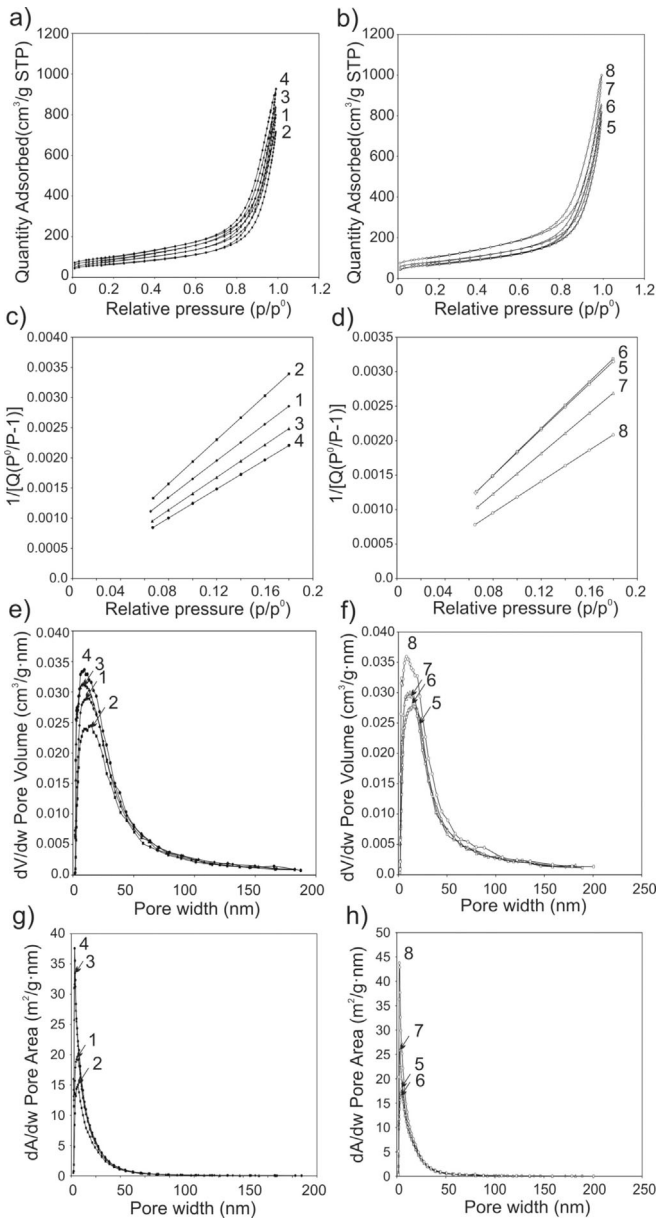

Figure 6. (a) Adsorption/desorption isotherms, (b–d) BET surface area plot, (e,f) BJH adsorption dV/dw pore volume, (g,h) BJH adsorption dA/dw pore area of (1) NDs (◆), (2) 1150-CNOs (■), (3) 1450-CNOs (▲), (4) 1650-CNOs (•), (5) AM-NDs (◇), (6) 1150-N-CNOs (□), (7) 1450-N-CNOs (Δ), and (8) 1650-N-CNOs (°).

tained for NDs and AM-NDs annealed at 1650 °C, 454 $m^2 g^{-1}$ for plain CNOs and 383 $m^2 g^{-1}$ for N-CNOs, respectively (Table 2). The total surface area is conventionally divided into two parts, the micropore surface area and the external surface area, that is equivalent to the mesopore surface area.[10]

According to the IUPAC classification, pores can be classified into three groups according to their size: micropores (<2 nm), mesopores (between 2 and 50 nm) and macropores (larger than 50 nm).[10] Comparison of the porous properties of the materials allowed to state the following conclusions: (i) both nanostructures (non-modified and nitrogen-doped) have mainly mesoporous morphologies with pores in the 2≈50 nm diameter range (according to the pore size distribution curves of the Barret–Joyner–Halenda (BJH) adsorption); (ii) there is also a small fraction of micropores (<2 nm) available in all of the CNO materials; (iii) the nitrogen-doped CNOs (0.0262 $cm^3 g^{-1}$) have a higher content of micropores compared to undoped nanostructures (0.0195 $cm^3 g^{-1}$); and (iv) annealing of NDs and AM-NDs at higher temperatures led to more porous structures with higher content of micropore domains.

Average pore sizes were also estimated from the pore volume, which is derived from the amount of N_2 gas adsorbed at a relative pressure close to unity (t-Plot method and BJH model). It was observed that the average pore size of ≈17 nm for NDs did change significantly during the annealing process and formation of undoped CNOs (≈12 nm) (Table 2). Annealing of AM-NDs, led to lowers pore sizes from 18 (AM-NDs) to 16 nm (1650-N-CNOs). It is known that the surface area of carbon materials accessed by nitrogen gas is also available for electrolyte access in aqueous solutions and the micropore surface area has the same electroadsorption properties as that of the external surface area. Therefore, there should be a correlation between the textural properties and the electrochemical properties of carbon materials.

Electrochemical and electrocatalytic properties of CNOs and N-CNOs

To explore the potential application of the materials in energy storage devices, the samples were used as supercapacitor electrodes and characterized using cyclic voltammetry (CV), galvanostatic charge/discharge measurements and electrochemical impedance spectroscopy (EIS) in 1 mol dm^{-3} H_2SO_4 and NaOH aqueous solution (Figures 7, S3–S6). Capacitance measurements were performed by three techniques (cyclic voltammetry, galvanostatic charge/discharge and impedance spectrosco-

Table 2. Best-fit frequencies for *D*, *G* and *2D* bands obtained at 514 nm laser excitation energies and relative intensity I_D/I_G and I_{2D}/I_G.

Sample	S_{BET} [a] [$m^2 g^{-1}$]	S_{ext} [b] [$m^2 g^{-1}$]	Pore volume [V_p, $cm^3 g^{-1}$][c]	Micropore volume [V_p, $cm^3 g^{-1}$][d]	Pore size [nm][e]
NDs	285	269	1.231[f]	0.0068	17
1150-CNOs	235	214	1.099[g]	0.0108	19
1450-CNOs	322	288	1.289[h]	0.0171	16
1650-CNOs	454	408	1.660[i]	0.0195	12
AM-NDs	261	253	1.200[j]	0.0009	18
1150-N-CNOs	255	242	1.261[k]	0.0056	19
1450-N-CNOs	296	258	1.315[l]	0.0189	18
1650-N-CNOs	383	328	1.534[m]	0.0262	16

[a] S_{BET}—BET specific surface area. [b] S_{ext}—external surface area, based on t-plot method. [c] Based on BJH adsorption method. [d] Based on t-plot method. [e] Based on BJH adsorption method (4 V/A). Single point adsorption total pore volume of pores less than: [f] 1390 Å diameter at p/p^o = 0.9862; [g] 1373 Å diameter at p/p^o = 0.9860; [h] 1293 Å diameter at p/p^o = 0.9851; [i] 1193 Å diameter at p/p^o = 0.9836; [j] 1313 Å diameter at p/p^o = 0.9854; [k] 1323 Å diameter at p/p^o = 0.9855; [l] 1459 Å diameter at p/p^o = 0.9868; [m] 1466 Å diameter at p/p^o = 0.9869.

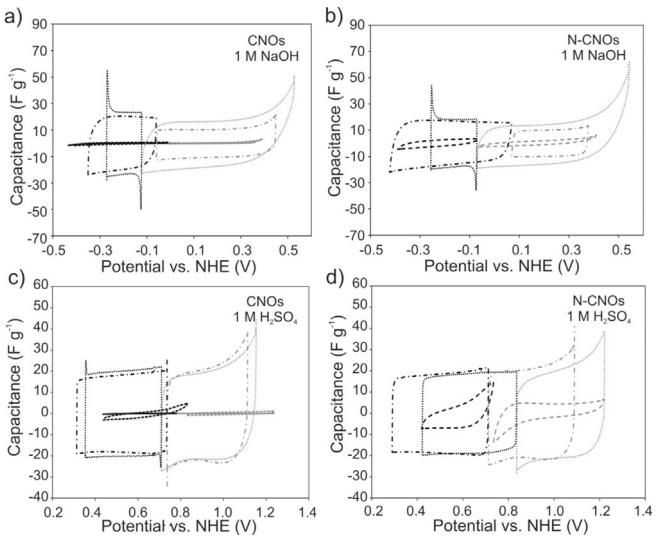

Figure 7. CV curves at a scan rate 5 mV s^{-1} in (a, b) 1 M NaOH and (c, d) 1 M H_2SO_4. Negative electrodes (black line) and positive electrodes (gray line) in three electrode cell. NDs (solid line), 1150-CNOs and 1150-N-CNOs (dashed line), 1450-CNOs and 1450-N-CNOs (dots line), and 1650-CNOs and 1650-N-CNOs (dashed and dots line).

py) in aqueous solutions. The specific capacitances (C_s) of the CNOs and their reference materials using cyclic voltammetry (CV) were determined based on the following Equation (1):

$$C_S = \frac{\int_{E_2}^{E_1} i(E)dE}{vm(E_1 - E_2)} \quad (1)$$

where E_1, E_2 are the initial and final potentials (V) respectively, $\int_{E_2}^{E_1} i(E)dE$ is the integrated current in the potential window, v is the sweep rate (V s^{-1}), and m is the mass of the active material. The specific capacitance (per electrode) was also evaluated by galvanostatic charge-discharge measurements, based on Equation (2):

$$C_S = \frac{2I\Delta t}{m\Delta U} \quad (2)$$

The CV measurements of the undoped and the N-doped CNO electrodes were performed using a three-electrode cell (Figure 7). All the CV curves obtained for the materials annealed at temperatures higher than 1450 °C show pseudorectangular profiles, indicating nearly ideal EDLC behavior. It was found that doping slightly decreases the capacitance for the negative and for the positive electrodes in 1 mol dm^{-3} NaOH (Figure 7). CNOs and the N-CNOs exhibit excellent capacitive behavior even under quick charge-discharge conditions. The following conclusions can be drawn: (i) the carbon nanostructures (undoped and N-doped) showed always the higher specific capacitance in acidic medium than in alkaline one; (ii) there is a gradual decrease in the specific capacitances with increasing sweep rates for all electrodes; (iii) when the sweep rate was increased from 1 to 100 mV s^{-1}, the capacitive current decreased to c.a. 80% (1650-CNOs and 1650-N-CNOs) of the starting value; (iv) significant decrease of the capacitive current was observed for sweep rates ca. 500 mV s^{-1} (c.a. 60% for undoped CNOs and c.a. 30% for nitrogen-doped CNOs). These results show that undoped CNOs had better cycling stability compared with the nitrogen-doped samples.

Figure S3 shows the charge-discharge curves of pristine and nitrogen-doped CNOs in 1 mol dm^{-3} H_2SO_4 at a current density of 100 mA g^{-1}. Analogous studies were also performed in 1 mol dm^{-3} NaOH (Figure S4). These reasonably symmetric and linear curves indicate good capacitive behavior. It should be noted that the specific capacitance of 1650-CNOs and 1650-N-CNOs are 20 and 17 F g^{-1} at 0.1 A g^{-1} (1 mol dm^{-3} H_2SO_4), respectively, which agrees well with the results obtained by cyclic voltammetry and electrochemical impedance spectroscopy. The lower values of specific capacitances were obtained in 1 mol dm^{-3} NaOH (14 and 12 F g^{-1} at 0.1 A g^{-1} for 1650-CNOs and 1650-N-CNOs, respectively).

Although the electrochemical characterization of doped carbon nanostructures indicates a slight degradation of some electrochemical parameters, substitution of nitrogen atoms in graphitic layers makes it possible to use these nanostructures in electrocatalysis. We have modified a glassy carbon electrode (GCE) with CNOs or N-CNOs to obtain a novel sensing platform for the non-enzymatic detection of hydrogen peroxide. The electrochemical properties of CNOs and N-CNOs were investigated by CV measurements. The potential application of N-CNOs/GCE was investigated by its performance for reduction of H_2O_2 compared with the CNOs modified GCE electrode in a three-electrode cell (working electrode: GCE, reference: Ag/AgCl and counter: Pt). Figures 8 and S7 show the CVs of N-CNOs/GCE and CNOs/GCE (carbon nanostructures obtained at different temperatures: 1150; 1450 and 1650 °C) in the absence and presence of H_2O_2 in the phosphate buffer solution (pH 7.4) at scan rates of 10 mV s^{-1}.

Hydrogen peroxide can undergo catalytic decomposition via reaction (3) or by self-dissociation in aqueous media by Equation (4):[52]

$$H_2O_2 \rightarrow H_2O + \frac{1}{2}O_2 \quad (3)$$

$$H_2O_2 \rightarrow 2H^+ + O_2^{2-} \quad (4)$$

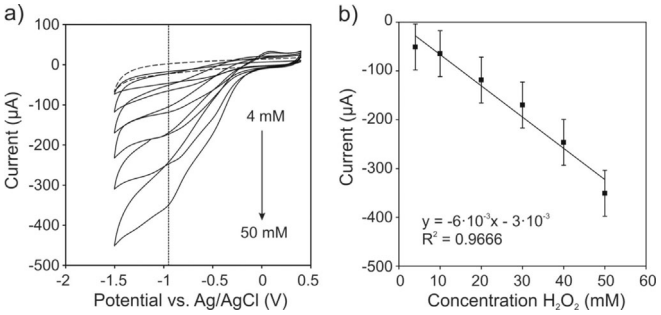

Figure 8. (a) CV curves of a GCE covered with 1650-N-CNOs in 0.01 M PBS (pH 7.4) with the absence (dashed black curves) and presence (solid black curves) of H_2O_2 with different concentrations (4, 10, 20, 30, 40, 50 mM) at a scan rate of 10 mV s^{-1}. (b) Dependence of reduction peak current on the H_2O_2 concentration.

Analysis of the CVs presented in Figure 8 allowed the following conclusions: (i) no obvious electrochemical reduction peak was observed at a bare GCE when hydrogen peroxide was added; (ii) the nitrogen-doped samples have a higher catalytic activity than the undoped prepared at the same temperatures; (iii) the highest electrocatalytic activity was observed for the samples prepared at 1650 °C; (iv) linear increases of reduction currents were observed with increasing H_2O_2 concentrations from 4 to 50 mmol dm^{-3}; and (v) the reduction of H_2O_2 also occurs at lower overpotentials with N-CNOs than at undoped CNOs. Our research indicates that nitrogen-doping of CNOs is a simple method to increase their electrocatalytic properties.

Conclusions

In summary, we have shown that annealing of aminated-nanodiamond particles under an inert He atmosphere resulted in the formation of nitrogen-doped carbon nano-onions. Transmission electron microscopy results indicate that the nitrogen-doped nanostructures have polyhedral structures rather than spherical, a direct confirmation of the substitution of some carbon atoms by nitrogens in the layers. One of the advantages of this method is the possibility of substitution of carbon atoms on the entire structure of the CNOs, which leads to structural modifications of whole nanoparticles rather than just their surfaces. This method maintains the π-conductive surface of CNOs, which is crucial for their applications in electrochemistry and electronics. The main advantage of these materials is their use as electroactive materials in non-enzymatic electrocatalytic reactions.

Experimental Section

Materials

All chemicals and solvents used were commercially available and used without further purification: nanodiamond powder (NDs, Carbodeon μDiamond®Molto) and aminated-nanodiamond (AM-NDs, Carbodeon μDiamond®Amine P; surface contained nitrogen, according to Kjeldahl method ≥2000 mg kg^{-1}; both carbon nanostructures had crystal sizes between 4–6 nm and content larger than 97 wt.%, sodium chloride (≈98%, Sigma–Aldrich), anhydrous ethanol (99.8%, POCh, Poland), phosphate buffered saline (PBS) powder pH 7.4 (Sigma–Aldrich), sulfuric acid (puriss. p.a. 95–97%, POCH, Poland), sodium hydroxide (pellets, >98%, Sigma–Aldrich), hydrogen peroxide solution (>30%, Sigma–Aldrich). All aqueous solutions for electrochemical studies were made using deionized water, which was further purified with the Milli-Q system (Millipore).

Synthetic procedures

Pristine CNOs (CNOs) and nitrogen-doped CNOs (N-CNOs): Commercially available pristine nanodiamond powder or aminated-nanodiamond powder with a crystal size between 4–6 nm was used for the preparation of CNOs or N-CNOs, respectively. Annealing of the ultradispersed NDs or AM-NDs was performed at 1150; 1450 and 1650 °C under a 1.1 MPa He atmosphere with a heating rate of 20 °C min^{-1} (an Astro carbonization furnace). The final temperature was maintained for one hour, then the material was slowly cooled to room temperature over a period of one hour. The furnace was opened, and the CNOs or N-CNOs were annealed in air at 400 °C to remove amorphous carbon.

Methods

The films were imaged by secondary electron scanning electron microscopy (SEM) using a FEI Tecnai S-3000N (Tokyo, Japan). The accelerating voltage of the electron beam was 20–30 keV. TEM imaging was performed at FEI Talos F200X device which is a high-resolution analytical transmission electron microscope, operated at 200 keV. This microscope is equipped with an X-FEG electron source module. This high source brightness enables near diffraction limited imaging and improves the spectroscopic performance. Moreover, Talos f200x is equipped with a four-quadrant 0.9-sr energy dispersive X-ray spectrometer (EDS) for elemental and compositional mapping.

Thermogravimetric experiments were performed using SDT 2960 Simultaneous TGA-DTG (TA Instruments company). The thermogravimetric spectra were recorded at 10 °C min^{-1} in air (100 mL min^{-1}). The powder diffraction data were measured at 293 K using a SuperNova diffractometer (Agilent) with a CCD detector and a $Cu_{K\alpha}$ radiation source at the 148 mm sample-to-detector distance. Prior to the experiment, all samples were loaded into capillaries with a diameter of 0.5 mm. N_2 gas adsorption measurements were performed using a Micromeritics apparatus (ASAP2020—automatic sorption analyser, Micromeritics Corp., USA) at −196 °C. Prior to gas adsorption analysis, all samples were degassed at 350 °C and 10 μmHg vacuum for 20 h to remove any adsorbed species.

The room temperature Raman spectra in the range between 100 and 3500 cm^{-1} were investigated with a Renishaw Raman InVia Microscope equipped with a high sensitivity ultra-low noise CCD detector. The radiation from an argon ion laser (514 nm) at an incident power of 1.15 mW was used as the excitation source. Raman spectra were acquired with 3 accumulations of 10 s each, 2400 L mm^{-1} grating and using a 20x objective. The Fourier Transform Infrared (FTIR) spectra were recorded in the range between 4000 and 100 cm^{-1} with a Nicolet 6700 Thermo Scientific spectrometer at room temperature under a N_2 atmosphere. The spectra were collected at a resolution of 4 cm^{-1}, apodized with a triangular function, and a zero-filling factor of 1 was applied. All the spectra were corrected with conventional software in order to cancel the variation of the analyzed thickness with the wavelength.

For electrochemical studies, the capacitors were assembled in Swagelok®type cells by using two electrodes and fiber glass material as a separator. The pellets for electrochemical measurements consisted of 85% of the active electrode material, 10% of binder (polyvinylidene fluoride, PVDF Kynar Flex 2801) and 5% of acetylene black (Super C65, IMERYS). The mass of the electrodes was in the range of 8 to 10 mg and a geometric surface area of 0.8 cm^2. 1 mol dm^{-3} H_2SO_4 or NaOH was used as an electrolyte for electrochemical measurements. All potentials were measured using three-electrode configurations and are reported versus the normal hydrogen electrode (NHE). All capacitors were examined using cycling voltammetry (1–100 mV s^{-1}), galvanostatic cycling and electrochemical impedance spectroscopy (100 kHz–1 mHz) using a VMP3 Biologic.

The electrochemical measurements (electrocatalytic studies) were performed using a computer-controlled Autolab modular electrochemical system equipped with a PGSTAT 12 potentiostat (Eco Chemie Utrecht, The Netherlands), using the NOVA 1.7 software (Eco Chemie Utrecht) and a three-electrode cell configuration. The working electrode was a glassy carbon (GC) disk electrode (Bioana-

lytical System Inc.) with a disk diameter of 2.0 mm. Prior to the measurements, the surface of the glassy carbon electrode was polished using 3.0 μm fine diamond polish and 1.0 μm micropolish alumina (Buehler) on Texmet/alumina pad (BASi). Afterwards, the GC electrode was immersed in ethanol, sonicated for a few minutes to remove the traces of alumina from the surface, washed with ethanol and dried. The film on the GC electrode was prepared as follows: 2 mg of an active material was dissolved in a solution containing conductive carbon paint and ethanol in a volume ratio of 1:6 and sonicated for 15 minutes. Subsequently, the surface of the working electrode was modified by the drop-coating method. 10 μL of the CNOs or N-CNOs solution were transferred to the GC (1.5 mm diameter) surface and the solvent was evaporated under an argon atmosphere. A saturated calomel electrode was used as reference electrode. The counter electrode was made from platinum mesh (0.25 mm). All experiments were done in water purified in a Millipore apparatus and saturated with argon.

Acknowledgements

We gratefully acknowledge the financial support of the National Science Centre, Poland (grant #2012/05/E/ST5/03800) to M.E.P.-B. L.E. thanks the Robert A. Welch Foundation for an endowed chair, grant #AH-0033 and the US NSF, grants: PREM program (DMR-1205302) and CHE-1408865. SEM, XRD, porosimeter, Raman and FTIR were funded by European Funds for Regional Development and National Funds of Ministry of Science and Higher Education, as part of the Operational Programme Development of Eastern Poland 2007–2013, projects: POPW.01.03.00-20-034/09 and POPW.01.03.00-20-004/11.

Conflict of interest

The authors declare no conflict of interest.

Keywords: carbon nano-onion · doping · electrocatalysis · nitrogen

[1] J. Bartelmess, S. Giordani, *Beilstein J. Nanotechnol.* **2014**, *5*, 1980.
[2] R. Bacon, *J. Appl. Phys.* **1960**, *31*, 283.
[3] V. L. Kuznetsov, A. L. Chuvilin, Y. V. Butenko, I. Y. Mal'kov, V. M. Titov, *Chem. Phys. Lett.* **1994**, *222*, 343.
[4] L. G. Bulusheva, A. V. Okotrub, V. L. Kuznetsov, D. V. Vyalikh, *Diamond Relat. Mater.* **2007**, *16*, 1222.
[5] K. N. Wood, R. O'Hayre, S. Pylypenko, *Energy Environ. Sci.* **2014**, *7*, 1212.
[6] Y. Gogotsi, D. Guldi, R. McCreery, C.-C. Hu, C. Merlet, F. Béguin, L. Hardwick, E. Frackowiak, J. Macpherson, A. Forse, G. Z. Chen, K. Holt, R. Dryfe, H. Kurig, S. Sharma, P. R. Unwin, T. Rabbow, W. Yu, F. Qiu, F. Juarez, C. Sole, B. Dyatkin, K. Stevenson, Y. Cao, N. Cousens, A. Noofeli, *Faraday Discuss.* **2014**, *172*, 239.
[7] E. Frackowiak, *Phys. Chem. Chem. Phys.* **2007**, *9*, 1774.
[8] F. Béguin, V. Presser, A. Balducci, E. Frackowiak, *Adv. Mater.* **2014**, *26*, 2219.
[9] M. Rajkumar, C.-T. Hsu, T.-H. Wu, M.-G. Chen, C.-C. Hu, *Prog. Nat. Sci. Mater. Int.* **2015**, *25*, 527.
[10] H. Shi, *Electrochim. Acta* **1996**, *41*, 1633.
[11] J. Zhang, M. Terrones, C. R. Park, R. Mukherjee, M. Monthioux, N. Koratkar, Y. S. Kim, R. Hurt, E. Frackowiak, T. Enoki, Y. Chen, Y. Chen, A. Bianco, *Carbon* **2016**, *98*, 708.
[12] K. Kierzek, E. Frackowiak, G. Lota, G. Gryglewicz, J. Machnikowski, *Electrochim. Acta* **2004**, *49*, 515.
[13] H.-H. Chang, C.-K. Chang, Y.-C. Tsai, C.-S. Liao, *Carbon* **2012**, *50*, 2331.
[14] K. Fic, G. Lota, E. Frackowiak, *Electrochim. Acta* **2010**, *55*, 7484.
[15] D. Gastol, J. Walkowiak, K. Fic, E. Frackowiak, *J. Power Sources* **2016**, *326*, 587.
[16] G. Lota, B. Grzyb, H. Machnikowska, J. Machnikowski, E. Frackowiak, *Chem. Phys. Lett.* **2005**, *404*, 53.
[17] L. G. Bulusheva, A. V. Okotrub, A. G. Kurenya, H. Zhang, H. Zhang, X. Chen, H. Song, *Carbon* **2011**, *49*, 4013.
[18] G. A. Ferrero, K. Preuss, A. Marinovic, A. B. Jorge, N. Mansor, D. J. L. Brett, A. B. Fuertes, M. Sevilla, M.-M. Titirici, *ACS Nano* **2016**, *10*, 5922.
[19] M. Blanco, P. Álvarez, C. Blanco, M. V. Jiménez, J. J. Pérez-Torrente, L. A. Oro, J. Blasco, V. Cuartero, R. Menéndez, *Catal. Sci. Technol.* **2016**, *6*, 5504.
[20] B. Nagy, S. Villar-Rodil, J. M. D. Tascón, I. Bakos, K. László, *Microporous Mesoporous Mater.* **2016**, *230*, 135.
[21] X. Bo, M. Zhou, L. Guo, *Biosens. Bioelectron.* **2017**, *89*, 167.
[22] P. Wu, P. Du, H. Zhang, C. Cai, *Phys. Chem. Chem. Phys.* **2013**, *15*, 6920.
[23] X. Xu, S. Jiang, Z. Hu, S. Liu, *ACS Nano* **2010**, *4*, 4292.
[24] S. G. Rhee, *Science* **2006**, *312*, 1882.
[25] N. Narayanaswamy, S. Narra, R. R. Nair, D. K. Saini, P. Kondaiah, T. Govindaraju, *Chem. Sci.* **2016**, *7*, 2832.
[26] G. Wu, C. Dai, D. Wang, D. Li, N. Li, *J. Mater. Chem.* **2010**, *20*, 3059.
[27] G. Wu, M. Nelson, S. Ma, H. Meng, G. Cui, P. K. Shen, *Carbon* **2011**, *49*, 3972.
[28] N. Wu, X. Liu, S. W. Or, *AIP Adv.* **2016**, *6*, 056206.
[29] C. Zhu, F. Xu, J. Chen, H. Min, H. Dong, L. Tong, K. Qasim, S. Li, L. Sun, *J. Power Sources* **2016**, *303*, 159.
[30] Y. Lin, X. Pan, W. Qi, B. Zhang, D. S. Su, *J. Mater. Chem. A* **2014**, *2*, 12475.
[31] S. Tomita, M. Fujii, S. Hayashi, *Phys. Rev. B* **2002**, *66*, 245424.
[32] S. Tomita, A. Burian, J. C. Dore, D. LeBolloch, M. Fujii, S. Hayashi, *Carbon* **2002**, *40*, 1469.
[33] A. E. Aleksenskii, M. V. Baidakova, A. Y. Vul", V. Y. Davydov, Y. A. Pevtsova, *Phys. Solid State* **1997**, *39*, 1007.
[34] Q.-H. Yang, P.-X. Hou, M. Unno, S. Yamauchi, R. Saito, T. Kyotani, *Nano Lett.* **2005**, *5*, 2465.
[35] S.-W. Bian, Z. Ma, W.-G. Song, *J. Phys. Chem. C* **2009**, *113*, 8668.
[36] A. Vinu, P. Srinivasu, D. P. Sawant, T. Mori, K. Ariga, J.-S. Chang, S.-H. Jhung, V. V. Balasubramanian, Y. K. Hwang, *Chem. Mater.* **2007**, *19*, 4367.
[37] V. N. Mochalin, O. Shenderova, D. Ho, Y. Gogotsi, *Nat. Nanotechnol.* **2011**, *7*, 11.
[38] A. Jorio, A. G. Souza Filho, *Annu. Rev. Mater. Res.* **2016**, *46*, 357.
[39] D. Roy, M. Chhowalla, H. Wang, N. Sano, I. Alexandrou, T.. Clyne, G. A.. Amaratunga, *Chem. Phys. Lett.* **2003**, *373*, 52.
[40] S. Maldonado, S. Morin, K. J. Stevenson, *Carbon* **2006**, *44*, 1429.
[41] A. Aleksenskiy, M. Baidakova, V. Osipov, A. Vul" in *Nanodiamonds* (Ed.: D. Ho), Springer US, Boston, MA, 2010; pp. 55 – 77.
[42] A. Krueger, *J. Mater. Chem.* **2008**, *18*, 1485.
[43] V. Mochalin, S. Osswald, Y. Gogotsi, *Chem. Mater.* **2009**, *21*, 273.
[44] A. K. M. S. Chowdhury, D. C. Cameron, M. S. J. Hashmi, *Thin Solid Films* **1998**, *332*, 62.
[45] S. Kumar, T. L. Tansley, *Thin Solid Films* **1995**, *256*, 44.
[46] M. Rusop, T. Soga, T. Jimbo, *J. Mater. Sci. Mater. Electron.* **2005**, *16*, 365.
[47] S. Prawer, K. Nugent, D. Jamieson, J. Orwa, L. Bursill, J. Peng, *Chem. Phys. Lett.* **2000**, *332*, 93.
[48] J. H. Kaufman, S. Metin, D. D. Saperstein, *Phys. Rev. B* **1989**, *39*, 13053.
[49] B. C. Smith, *Infrared spectral interpretation: a systematic approach*, CRC Press, Boca Raton, **1999**.
[50] M. Khavarian, S. P. Chai, S. H. Tan, A. R. Mohamed, *J. Appl. Sci.* **2011**, *11*, 2382.
[51] C. Wu, Q. Guo, P. Yin, T. Li, Q. Yang, Y. Xie, *J. Phys. Chem. B* **2005**, *109*, 2597.
[52] J. D. Gaynor, A. S. Karakoti, T. Inerbaev, S. Sanghavi, P. Nachimuthu, V. Shutthanandan, S. Seal, S. Thevuthasan, *J. Mater. Chem. B* **2013**, *1*, 3443.

Manuscript received: June 19, 2017
Accepted manuscript online: June 21, 2017
Version of record online: ■■ ■■, 0000

FULL PAPER

Annealing aminated nanodiamond particles under an inert He atmosphere resulted in the formation of nitrogen-doped CNOs. One of the advantages of this method is the possibility of substitution of carbon atoms on the entire structure of the CNOs, which leads to structural modifications of whole nanoparticles rather than just their surfaces. Nitrogen-doped CNOs have a high catalytic activity in non-enzymatic reactions.

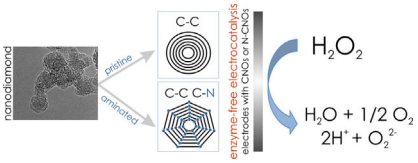

Carbon Nanostructures

*Olena Mykhailiv, Halyna Zubyk, Krzysztof Brzezinski, Malgorzata Gras, Grzegorz Lota, Marianna Gniadek, Elkin Romero, Luis Echegoyen, Marta E. Plonska-Brzezinska**

■■ – ■■

Improvement of the Structural and Chemical Properties of Carbon Nano-onions for Electrocatalysis